INVESTIGATION ON THE FLUIDIZATION DYNAMICS OF COHESIVE GELDART B PARTICLES USING X-RAY TOMOGRAPHY AND PRESSURE FLUCTUATION ANALYSIS

Jiliang Ma[1*], J. Ruud van Ommen[2], Daoyin Liu[1], Robert F. Mudde[2], Xiaoping Chen[1], Cai Liang[1]

[1] *Key Laboratory of Energy Thermal Conversion and Control of Ministry of Education, School of Energy and Environment, Southeast University, Nanjing 210096, P.R. China*

[2] *Product & Process Engineering, Department of Chemical Engineering, Delft University of Technology, van der Maasweg, 9, 2629 HZ, Delft, The Netherlands*

Abstract –In many applications of fluidized reactors, the particles processed are cohesive. The presence of inter-particle cohesive force causes different fluidization dynamics compared to non-cohesive system. This paper studied the fluidization dynamics of cohesive Geldart B particles in a three dimensional fluidized bed. X-ray tomography and in-bed pressure fluctuation analysis were conducted to reveal bubble behaviors as well as overall fluidization status. The results show that increasing cohesive force facilitates bubble coalescence, leading to the growth of bubble size. When bubbles grow to similar dimensions to the column cross section, the particles above bubbles are lifted as a particle slug and the fluidization turns to slugging. As the cohesive force increases, the energy distribution of power spectral density of pressure signal changes from mono-modal shape to bi-modal shape where two peaks relate to slugging and normal fluidization respectively. At low static bed heights, no slugging takes place even under high cohesive forces. Therefore, to avoid slugging in the practical application, the static bed height should be kept as low as possible. With further increase in the static bed heights, bubbles keep growing by continuous coalescence and become considerable near the bed surface, which triggers slugging and causes an increase in slugging duration.

INTRODUCTION

Fluidized beds are widely used in industrial processes for their vigorous heat and mass transfer and flexibility in handling particles continuously. In many applications of fluidized reactors, the particles processed are cohesive. The presence of inter-particle cohesive force causes different fluidization dynamics in comparison to non-cohesive system (Shabanian and Chaouki, 2017). Especially when the cohesive force is large enough, agglomeration takes place, leading to shut down of the process (Parise et al., 2011). Thus, it is attractive to address the underlying mechanisms, based on which, the manipulation of cohesive fluidized bed reactors could be optimized.

Cohesive force may exist in multiple forms, such as van der Waals force (Rietema et al., 1993), electrostatic force (Tamadondar et al., 2014), liquid bridge force (Li and Kato, 2001), and particle bridge force (Tardos and Pfeffer, 1995). The present paper focuses on the particle bridge force. Generally, increasing the operational temperature of fluidized bed processing low-melting particles (Seville et al., 1998) is a preferable approach to introduce particle bridge force. However, it requires the bed operated at high temperature, which reduces the measurement techniques applicable for such extreme conditions. Shabanian et al. (2011) presented a novel method to introduce cohesive force by coating inert particles with polymer materials whose cohesiveness is proportional to the temperature. At proper polymer layer thickness, the cohesive force between particles could be changed over a wide range, within a low degree of temperatures. Based on this, the effects of cohesive force on the particle trajectory and velocity, emulsion phase voidage, transition from bubbling to turbulent regime and pressure fluctuations in a fluidized bed were studied (Shabanian and Chaouki, 2014, 2015). Note that, the variation of fluidization dynamics with tenderly increasing cohesive force and the dynamical features before and after fluidization failure under considerably large cohesive force are still unknown. Therefore, further investigations are needed on this topic to reveal the complex flow structures in the cohesive bed.

This paper investigates the fluidization dynamics of cohesive Geldart B particles by combining X-ray tomography and in-bed pressure fluctuation analysis. We used the approach of "polymer coating" presented by Shabanian et al. (2011) to introduce inter-particle cohesive force. By controlling the bed temperature, the particle cohesiveness is adjusted over a wide range so that the evolution of fluidization from normal status to defluidization could be captured. The effects of cohesive force and static bed heights (H_s) on the fluidization dynamics at different measurement heights were carefully examined. Finally, we evaluated global defluidization characteristics with the cycle frequency of pressure signal and analysed how it changes with operational parameters.

EXPERIMENTAL DESCRIPTION

2.1 Experimental setup

The experiment was conducted in a Perspex column with an inner diameter of 0.14 m and height of 1.6 m as shown in Fig.1. Bed materials are heated by fluidizing air whose temperature is controlled by an electrical heater located in the air feeding line. Bed temperature was monitored through a thermal couple inserted in the bed at a height of 110 mm from gas distributor. Four probes, with 4 mm i.d. and 0.1 m length, were in-line installed with distances of 30 mm, 110 mm, 190 mm and 270 mm from gas distributor respectively. Each probe was equipped with a wire gauze to prevent particles from entering the probe. Four gauge pressure sensors of Kistler type 7261 were connected to the probes to measure in-bed pressure fluctuations. The charges from pressure sensors were then transmitted to amplifiers (Kistler amplifier type 5015) and converted to voltage signals which afterwards were stored using a National Instruments CompactRIO embedded control and acquisition system. Besides that, X-ray tomography developed at TU Delft was also performed to achieve the void distribution over the cross section of column. It was developed on the basis of Lambert-Beer law. Three X-ray sources were placed at 120° around the column. Each source generated a fan beam that was detected by a tube bank mounted opposite to the source. Each tube bank consisted of two detector arrays, creating two measuring planes separated by approximately 1.09 cm. Each array has 32 detectors, so there are 192 detectors in total. The column was placed on a lifting table so that the cross section at different heights (70 mm, 150 mm and 230 mm from the distributor) could be scanned by adjusting the table height. In order to minimize the harm to health caused by the radiation, the setup was located in a room whose walls are made of lead. The on-off operation of X-ray tomography and the data collection were controlled by the equipment located in another room. The data sampling for pressure signal and X-ray detector output were synchronized with LabView code. The pressure data was measured for 10 minutes with a sampling frequency of 1250 Hz, and the X-ray intensity was measured for 1 minute with a sampling frequency of 2500 Hz. By applying reconstruction algorithm to X-ray output, 3D version of bubbles crossing the measurement plane could be reconstructed, as shown in Fig.1. The experiments were performed at bed temperatures ranging from 25 °C to 50 °C with a step of 5 °C and fluidization gas velocities, U_g, from $2U_{mf}$ to $3U_{mf}$. Four static bed heights, H_s: 120 mm, 200 mm, 300 mm and 400 mm were studied.

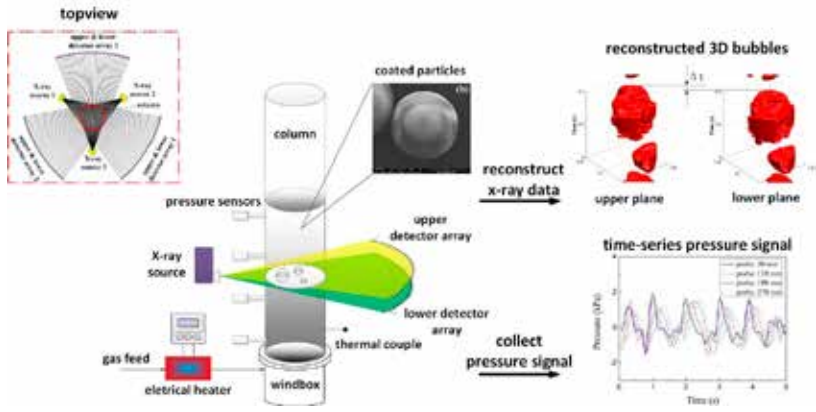

Fig.1 Schematic of experimental setup.

2.2 Materials

The inter-particle cohesive force was introduced by coating glass beads with a uniform polymer layer. The glass beads have a density of 2500 kg/m^3 and an average diameter of 600 μm. The minimum fluidization velocity of glass beads, U_{mf}, was measured to be 0.325 m/s. According to the classification of Geldart, they belong to group B particles. The polymer layer was the mixture of Poly ethyl acylate (PEA) and poly methyl methacrylate (PMMA) with a mass ratio of 2 to 1. Before coating, it was dissolved in the aqueous dispersion whose commercial name is Eudragit NE30D. In order to guarantee a good coating quality, the spray process for the present work was divided into four batches during which sufficient time was provided for distribution and solidification of polymer layer. Fig.2 shows the surface morphology of glass beads before and after coating on the basis of SEM analysis. In this study, the thickness of polymer layer was around 10 μm.

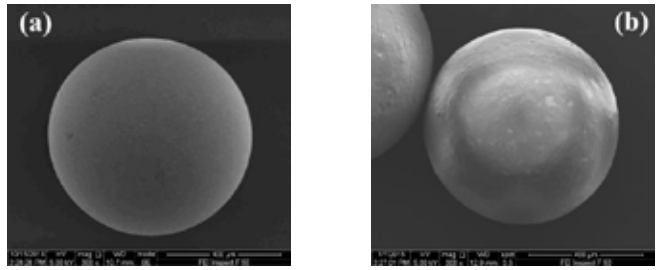

Fig.2 SEM images of the glass beads before and after coating.
(a) uncoated particle, (b) coated particle

RESULTS AND DISCUSSIONS

Fig.3 illustrates the reconstructed bubbles under different cohesive forces at the measurement heights of 70 mm, 150 mm and 230 mm respectively. Taking the height of 70 mm (Fig.3(a)) as an example, for the bed temperature of 30°C, bubbles are large in number but small in size. Moreover, there are multiple bubbles consisting of small bubbles connected to each other. As the cohesive force increases, the bubble number decreases, accompanied by the increase in bubble size. With further enhancement of bed temperature to 45°C, large bubbles with similar dimension to the cross section of column arise, converting normal fluidization to slugging. When slugging occurs, a piston-like movement of the bed as a whole (referred as particle slug) was observed. Once the particle slug breaks up, the bed collapses to a state free of bubbles and shows a periodicity in the formation of slugging. Due to frequent bubble coalescence, fewer but larger bubbles are observed at higher measurement plane. Note that, this feature seems unconspicous for the case of 45 °C: the bubbles at 230 mm are not larger than those measured at lower planes. This may be caused by the fact that the particle slug breaks before reaching such height. Later, we will extract quantitative information from reconstructed bubbles and confirm the rough observation. Because of the positive role of cohesive force in the growth of bubbles, it can be inferred that the specific area of bubbles decreases with increasing cohesive force, thereby causing the deterioration of mass transfer between emulsion phase and bubble phase.

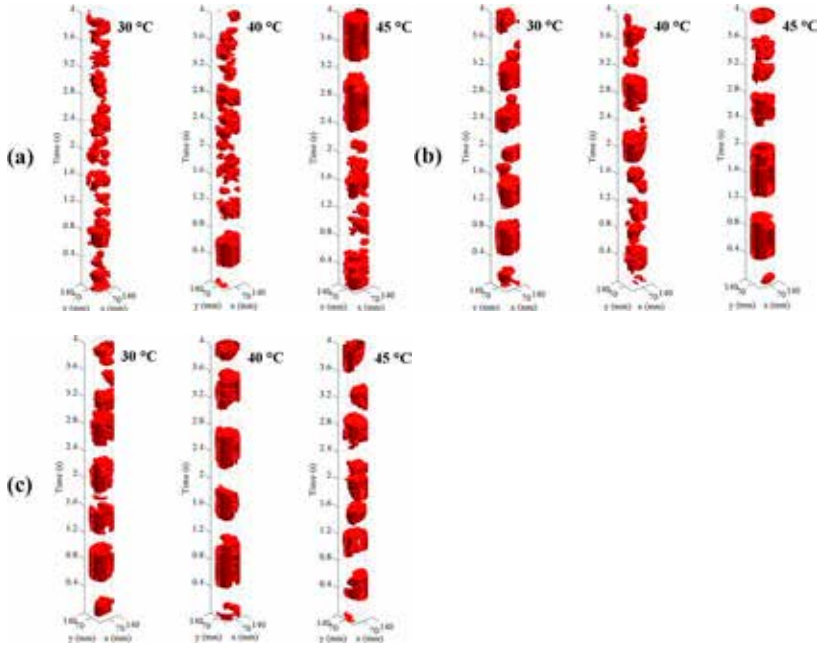

Fig.3 Reconstructed bubbles under different cohesive forces.

Static bed height: 300 mm; fluidization velocity: U_g=2.5U_{mf}; measurement heights: (a) 70 mm, (b) 150 mm, (c) 230 mm.

Fig.4 shows the power spectral density (PSD) of pressure fluctuation measured at different positions and cohesive forces. For the bed temperature of 30 °C, the PSD curve is generally mono-modal shape with a dominant peak around 1 Hz that is usually considered as the natural oscillation frequency of the bed (Sasic et al., 2006, Hao and Bi, 2005). Thus it is inferred that the pressure waves generated by the bed oscillation may dominant pressure fluctuations. Besides the dominant peak, other distinct peaks with less energy are also observed, relating to the rupture of large bubbles into smaller ones or the formation of multi-bubble structure of the bed (Azizpour et al., 2012). With the presence of larger cohesive force, the PSD curve changes from mono-modal shape to bi-modal shape. The low-frequency peak appears at around 0.1 Hz and the high-frequency peak locates in the range of 0.8 to 1.6 Hz. Basically, the low-frequency peak relates to intermittently occurring slugging as introduced in Fig.3. Different from the slugging of non-cohesive bed where the PSD curve shows a distinct and narrow-bandwidth peak (Jaiboon et al., 2013, Shou and Leu, 2005), the PSD curve for the cohesive bed has two peaks relating to slugging and normal fluidization respectively due to the alternative process between these two statuses. That is why the intensity peak for the slugging corresponds to such a low frequency of 0.1 Hz. As the cohesive force increases, the PSD curve has a broader band of peak frequencies, suggesting an intensified multiple-bubbling fluidization (Jaiboon et al., 2013), and the curve shifts toward smaller frequencies, indicating a decline of bubble numbers. The intensity of low-frequency peak increases with cohesive force, implying an increasing length of gas slug generated by the uprising particle slug. Moreover, the low-frequency peak intensity decreases with the elevation of measurement height. This behavior is opposite to the non-cohesive bed where the peak intensity for slugging increases with the measurement height due to increasing bubble size over coalescence (Jaiboon et al., 2013). The comparison between the intensities of two peaks at large cohesive force, e.g. 45 °C reveals that the intensity of low-frequency peak is much larger than the high-frequency peak for the signal measured near distributor (Fig.4(a)), implying the production of larger voids with smaller numbers. This difference decreases with the elevation of measurement height, indicating a gradual decline of the gas slug in comparison to the normal bubble sizes.

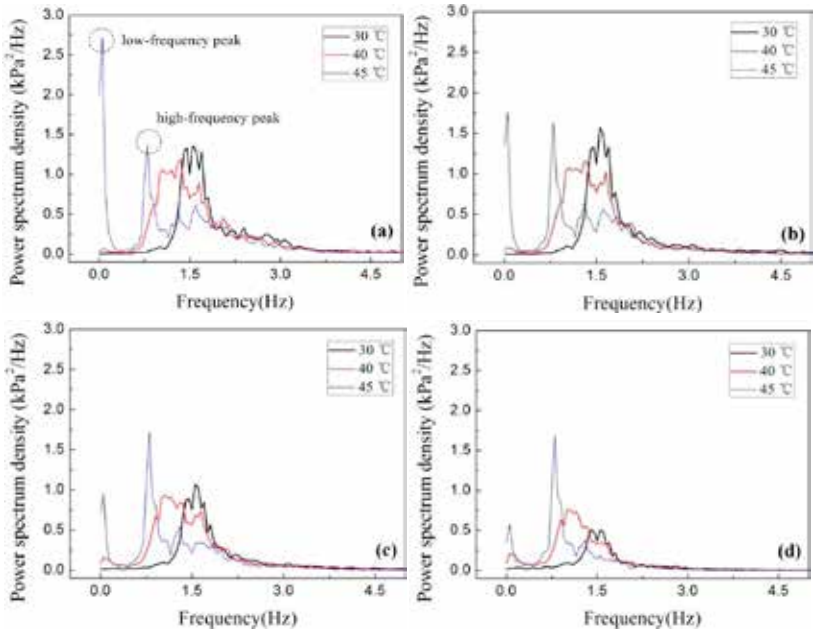

Fig.4 Power spectral density of pressure fluctuation at different heights and cohesive forces for U_g=2.5U_{mf}. measurement height: (a)30 mm; (b) 110 mm; (c) 190 mm; (d) 270 mm

Fig.5 shows the effects of cohesive force on the bubble frequency measured at different heights. Bubble frequency corresponds to the number of bubbles passing through the measurement plane per second. As can be seen, bubble frequency decreases with increasing cohesive force. Fig.6, plotting the equivalent diameter

of bubbles as a function of cohesive force, shows that bubble size increases with cohesive force. Combining the results of Fig.5 and Fig.6, it can be concluded that the presence of cohesive force facilitates the bubble coalescence. Moreover, the bubble number and bubble size at the measurement plane closer to the air distributor changes more apparent with cohesive force, indicating that the bubble coalescence near distributor is sensitive to cohesive force.

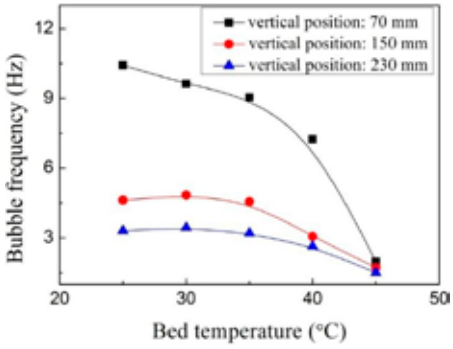

Fig.5 Bubble frequency at different measurement heights, as a function of cohesive force.

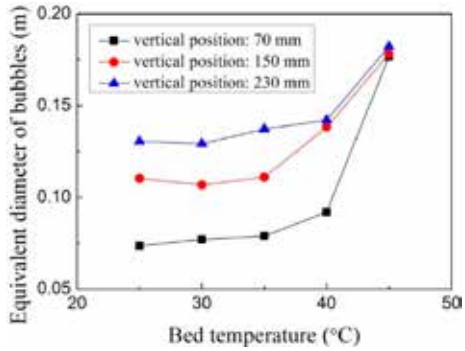

Fig.6 Equivalent bubble diameter at different measurement heights, as a function of cohesive force.

As introduced previously, when the cohesive force is large enough, the bed status is translated to an alternative process of normal fluidization and slugging, leading to the failure of fluidization. Therefore, a detailed understanding on the effects of various parameters on the slugging characteristics is valuable for the optimization of operation. Fig.7 plots an example of pressure fluctuation measured at 30 mm above distributor at the bed temperature of 45 °C. When slugging occurs, the pressure fluctuation curve is much more flat than normal fluidization. Aiming at quantifying the flatness of fluctuation curve, cycle frequency, f_c is an attractive choice for the ease of calculation. f_c is the number of times for the pressure curve crossing the average value per second. In this paper, we used f_c as the "threshold value" to evaluate the pressure signal section by section. The pressure signal over 10 minutes was divided into 600 sections so that each section is 1 s in length. f_c was calculated for each section. From rough observation, the cycle frequency for slugging is no larger than 2 Hz. Therefore, we used 2 Hz as the threshold value, below which, the evaluated section belongs to slugging (including 2 Hz). Based on this, the duration of slugging (t_s) and normal fluidization (t_n) are collected respectively. The slugging time fraction, $\tau_{slugging}$ was calculated as:

$$\tau_{slugging} = \frac{t_s}{t_s + t_n} \tag{1}$$

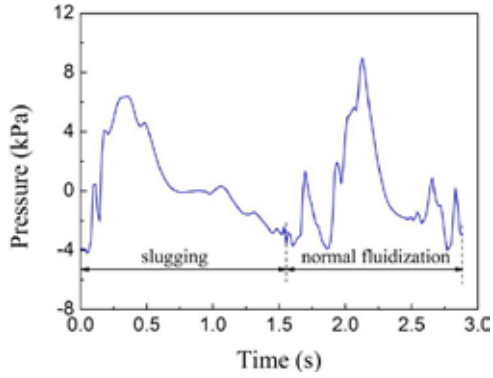

Fig.7 Time-series of pressure signals measured at 30 mm above distributor.

U_g=2.5U_{mf}, H_s=30 cm, bed temperature: 45 °C

Fig.8 shows the effect of static bed height on the variation of slugging time fraction with cohesive force. At the static bed heights of 120 mm and 200 mm, $\tau_{slugging}$ equals zero, indicating that no slugging takes place throughout the cohesive forces investigated. This is because the bubbles cannot fully develop due to the limitation of bed heights so that the bubble sizes are always smaller than the inner diameter of the column which would not trigger the formation of slugging. Therefore, to avoid slugging in practical applications, the static bed height should be kept as low as possible. Regarding the case of H_s=300 mm, the bubble size keeps growing by continuous coalescence and becomes considerable near bed surface, thereby causing slugging. Due to the considerable bubbles in the vicinity of bed surface, $\tau_{slugging}$ at the static bed height of 400 mm rises dramatically.

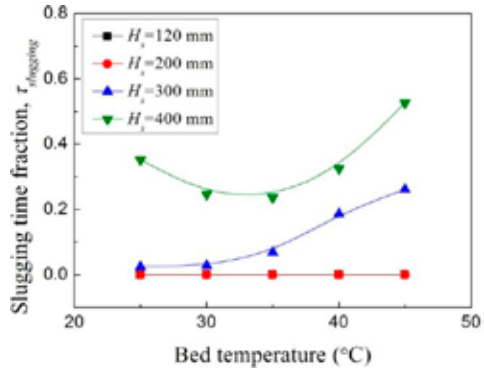

Fig.8 Slugging time fraction as a function of bed temperatures at U_g=2.5U_{mf} and measurement height of 30 mm.

CONCLUDING REMARKS

This paper investigates the hydrodynamics of a 3D column dealing with cohesive Geldart B particles based on pressure fluctuation analysis and X-ray tomography. The main conclusions are drawn as follows:

(1) The presence of cohesive force facilitates bubble coalescence which results in a decline of bubble frequency and an increase in the bubble size.

(2) When the cohesive force is large enough, the bed changes from normal status to an alternative process between normal fluidization and slugging.

(3) When slugging takes place, the fluctuation of in-bed pressure becomes more flat, which makes it possible to characterize the slugging with cycle frequency. Based on this, it is found that proper reduction in static bed height could suppress or even avoid slugging under large cohesive force.

ACKNOWLEDGEMENTS

We would like to acknowledge the financial support of this work by National Key Research and Development Plan (No.2016YFB0600802).

REFERENCES

Azizpour, H., Sotudeh-Gharebagh, R., Mostoufi, N., Zarghami, R. 2012. Characterization of regime transition in fluidized beds at high velocities by analysis of vibration signals. Industrial & Engineering Chemistry Research 51, 2855-2863.

Hao, B., Bi, H. T. 2005. Forced bed mass oscillations in gas-solid fluidized beds. Powder Technology 149, 51-60.

Jaiboon, O. A., Chalermsinsuwan, B., Mekasut, L., Piumsomboon, P. 2013. Effect of flow pattern on power spectral density of pressure fluctuation in various fluidization regimes. Powder Technology 233, 215-226.

Li, J., Kato, K. 2001. Effect of electrostatic and capillary forces on the elutriation of fine particles from a fluidized bed. Advanced Powder Technology 12, 187-205.

Parise, M. R., Silva, C. A. M., Ramazini, M. J., Taranto, O. P. 2011. Identification of defluidization in fluidized bed coating using the Gaussian spectral pressure distribution. Powder Technology 206, 149-153.

Rietema, K., Cottaar, E. J. E., Piepers, H. W. 1993. The effects of interparticle forces on the stability of gas-fluidized beds-II. Theoretical derivation of bed elasticity on the basis of van der Waal forces between powder particles. Chemical Engineering Science 48, 1687-1697.

Sasic, S., Leckner, B., Johnsson, F. 2006. Time-frequency investigation of different modes of bubble flow in a gas-solid fluidized bed. Chemical Engineering Journal 121, 27-35.

Seville, J. P. K., Silomon, H. P. Knight, P. C. 1998. Modelling of sintering in high temperature gas fluidization. Powder Technology 97: 160-169.

Shabanian, J., Fotovat, J., Chaouki, J., Bouffad, J. 2011. Fluidization behavior in a gas-solid fluidized bed with thermally induced inter-paticle forces, in: T. Knowlton (PSRI Eds.), 10th International Conference on Circulating Fluidized Beds and Fluidization Technology 2011: ECI Symposium Series, New York, pp. 738-745.

Shabanian, J., Chaouki, J. 2014. Local characterization of a gas-solid fluidized bed in the presence of thermally induced interparticle forces. Chemical Engineering Science 119, 261-273.

Shabanian, J., Chaouki, J. 2015. Hydrodynamics of a gas-solid fluidized bed with thermally induced interparticle forces. Chemical Engineering Journal 259, 135-152.

Shabanian, J., Chaouki, J. 2017. Effects of temperature, pressure, and interparticle forces on the hydrodynamics of a gas-solid fluidized bed. Chemical Engineering Journal 313, 580-590.

Shou, M. C., Leu, L. P. 2005. Energy of power spectral density fuction and wavelet analysis of absolute pressure fluctuation measurements in fluidized beds. Chemical Engineering Research & Design 83, 478-491.

Tamadondar, M. R., Zarghami, R., Tahmasebpoor, M., Mostoufi, N. 2014. Characterization of the bubbling fluidization of nanoparticles. Particuology 16, 75-83.

Tardos, G., Pfeffer, R. 1995. Chemical reaction induced agglomeration and defluidization of fluidized beds. Powder Technology 85, 29-35.